Eur. Phys. J. B **1**, 129–140 (1998)

THE EUROPEAN PHYSICAL JOURNAL B

Towards log-normal statistics in high Reynolds number turbulence

A. Arneodo[a], S. Manneville, and J.F. Muzy

Centre de Recherche Paul Pascal[b], Université Bordeaux I, avenue Schweitzer, 33600 Pessac, France

Received: 27 August 1997 / Accepted: 8 October 1997

Abstract. We report on the experimental application of a wavelet based deconvolution method that has been recently emphasized as a very efficient tool to extract some underlying multiplicative cascade process from synthetic turbulent signals. For high Reynolds number wind tunnel turbulence ($R_\lambda \simeq 2000$), using large velocity records (about 25×10^3 integral time scales), a cascading process is identified and found to be log-normal. This result relies on the Gaussian shape of the kernel $G_{aa'}$ that determines the nature of the cascade from a scale a' to a finer scale a. It is confirmed by investigating various standard quantities such as the probability density functions of the wavelet transform coefficients or the scaling exponents ζ_q that characterize the evolution across the scales of the moments of these distributions. Log-normal statistics are shown to hold on a well defined range of scales, that can be further used as an objective definition of the inertial range, and to depend on the Reynolds number. We comment on the asymptotic validity of the log-normal multifractal description.

PACS. 02.50.-r Probability theory, stochastic processes, and statistics – 47.27.Gs Isotropic turbulence; homogeneous turbulence – 47.27.Jv High-Reynolds-number turbulence

1 Introduction

Since Kolmogorov's founding work [1] (K41), fully developed turbulence has been intensively studied for more than fifty years [2–4]. A standard way to analyze a turbulent flow is to look for some universal statistical properties of the fluctuations of the longitudinal velocity increments over a distance l, $\delta v_l = v(x+l) - v(x)$. For instance, investigating the scaling properties of the structure functions:

$$S_p(l) = \langle |\delta v_l|^p \rangle \sim l^{\zeta_p}, \quad p > 0 \tag{1}$$

where $\langle \cdots \rangle$ stands for ensemble average, leads to a spectrum of scaling exponents ζ_p which has been widely used as a statistical characterization of turbulent fields [2–4]. Based upon the assumptions of statistical homogeneity and isotropy and of constant rate ϵ of energy transfer from large to small scales, the K41 theory [1] predicts the existence of an inertial range $\eta \ll l \ll L$ (η and L being respectively the dissipative and integral scales), where $S_p(l) \sim \epsilon^{p/3} l^{p/3}$. Although these assumptions are usually considered to be correct, there has been increasing numerical [5,6] and experimental [2–4,7–10] evidence that ζ_p deviates substantially from the K41 prediction $\zeta_p = p/3$, at large p. The observed nonlinear behavior of ζ_p is generally interpreted as a direct consequence of the intermittency phenomenon displayed by the rate of energy tranfer [11,12]. Under the so-called Kolmogorov's refined hypothesis [13], the velocity structure functions can be rewritten as $S_p(l) \sim \langle \epsilon_l^{p/3} \rangle l^{p/3} \sim l^{\tau(p/3)+p/3}$, where ϵ_l is the local rate of energy transfer over a volume of size l. The scaling exponents of S_p are thus related to those of the energy transfer: $\zeta_p = \tau(p/3) + p/3$.

Richardson's cascade pioneering picture [14] is often invoked to account for intermittency: energy is transferred from large eddies (of size of order L) down to small scales (of order η) through a cascade process in which the transfer rate at a given scale is not spatially homogeneous as in the K41 theory [1], but undergoes local intermittent fluctuations. Over the past thirty years, refined models including the log-normal model of Kolmogorov [13] and Obukhov [15] (KO62), multiplicative hierarchical cascade models like the random β-model, the α-model, the p-model (for review see Ref. [12]), the log-stable models [16, 17] and more recently the log-infinitely divisible cascade models [18–21] with the rather popular log-Poisson model advocated by She and Leveque [22] have overgrown in the literature as reasonable models to mimic the energy cascading process in turbulent flows. Unfortunately, all existing models appeal to adjustable parameters that are difficult to determine by plausible physical arguments and that generally provide enough freedom to account for the experimental data for the two sets of scaling exponents ζ_p and $\tau(p)$.

The scaling behavior of the velocity structure functions (Eq. (1)) is at the heart of the multifractal description

[a] e-mail: arneodo@crpp.u-bordeaux.fr
[b] CNRS UPR 8641

pioneered by Frisch and Parisi [23]. K41 theory [1] is actually based on the assumption that, at each point of the fluid, the velocity field has the same scaling behavior $\delta v_l(x) \sim l^{1/3}$, which yields the well-known $E(k) \sim k^{-5/3}$ energy spectrum. By interpreting the nonlinear behavior of ζ_p as a direct consequence of the existence of spatial fluctuations in the local regularity of the velocity field, $\delta v_l(x) \sim l^{h(x)}$, Frisch and Parisi [23] attempt to capture intermittency in a geometrical framework. For each h, let us call $D(h)$ the fractal dimension of the set for which $\delta v_l(x) \sim l^h$. By suitably inserting this local scaling behavior into equation (1), one can bridge the so-called singularity spectrum $D(h)$ and the set of scaling exponents ζ_p by a Legendre transform: $D(h) = \min_p(ph - \zeta_p + 1)$. From the properties of the Legendre transform, a nonlinear ζ_p spectrum is equivalent to the assumption that there is more than a single scaling exponent h. Let us note that from low to moderate Reynolds number turbulence, the inertial scaling range is uncomfortably small and the evaluation of ζ_p is not very accurate. Actually the existence of scaling laws like equation (1) for the structure functions is not clear experimentally [10,24] and this even at the highest accessible Reynolds numbers; this questions the validity of the multifractal description. Recently, Benzi *et al.* [25–27] have shown that one can remedy to the observed departure from scale-invariance by looking at the scaling behavior of one structure function against the other. More precisely, ζ_p can be estimated from the behavior $S_p(l) \sim S_3(l)^{\zeta_p}$, if one assumes that $\zeta(3) = 1$ [4]. The relevance of the so-called extended self-similarity (ESS) hypothesis is recognized to improve and to further extend the scaling behavior towards the dissipative range [5,25–27]. From the application of ESS, some experimental consensus has been reached on the definite nonlinear behavior of ζ_p and its possible universal character, at least as far as isotropic homogeneous turbulence is concerned [10]. But beyond some practical difficulties, there exists a more fundamental insufficiency in the determination of ζ_p. From the analogy [28] between the multifractal formalism and statistical thermodynamics, ζ_p plays the role of a thermodynamical potential which intrinsically contains only some degenerate information about the Hamiltonian of the problem, *i.e.*, the underlying cascading process. Therefore, it is not surprising that previous experimental determinations of the ζ_p spectrum have failed to provide a selective test to discriminate between various (deterministic or random) cascade models.

In order to go beyond the multifractal description, Castaing *et al.* [11,21,29–33] have proposed some approach of the intermittency phenomenon which relies on the validity of the Kolmogorov's refined hypothesis [13] and which consists in looking for a multiplicative cascade process directly on the velocity field. This approach amounts to model the evolution of the shape of the velocity increment pdf from Gaussian at large scales to more intermittent profiles with stretched exponential-like tails at smaller scales [8,11,34–36] by a functional equation that relates two scales using a kernel G. This description relies upon the ansatz that the velocity increment pdf at a given scale l, $P_l(\delta v)$, can be expressed as a weighted sum of dilated pdfs at a larger scale $l' > l$:

$$P_l(\delta v) = \int G_{ll'}(\ln \sigma)\, \frac{1}{\sigma}\, P_{l'}\left(\frac{\delta v}{\sigma}\right) \mathrm{d} \ln \sigma, \qquad (2)$$

where $G_{ll'}$ is a kernel that depends on l and l' only. Indeed most of the well-known cascade models can be reformulated within this approach [21,33]. This amounts (i) to specify the shape of the kernel $G(u)$ which is determined by the nature of the elementary step in the cascade and (ii) to define the way $G_{ll'}$ depends on both l and l'. In their original work, Castaing *et al.* [11,29–32] mainly focused on the estimate of the variance of G and its scale behavior. A generalization of Castaing *et al.* ansatz to the wavelet transform (WT) of the velocity field has been proposed in a previous paper [37] and shown to provide direct access to the entire shape of the kernel G. This wavelet based method has been tested on synthetic turbulent signals and preliminarily applied to turbulence data. The aim of the present study is to use this new method to process large velocity records in high Reynolds number turbulence. We start by briefly recalling our numerical method to estimate G. We then focus on the precise shape of G and show that, for the analyzed turbulent flow, G is Gaussian within a very good approximation. Special attention is paid to statistical convergence; in particular we show that when exploring larger samples than in previous studies [37–39], one is able to discriminate between log-normal and log-Poisson statistics. Going back to the WT coefficient pdf's and to the ζ_p spectrum, we eventually get additional confirmations of the relevance of log-normal statistics and discuss their robustness when varying the scale range or the Reynolds number. We conclude by discussing the asymptotic validity of the log-normal multifractal description of the intermittency phenomenon in fully developed turbulence.

2 Experimental evidence for log-normal cascading process in a high Reynolds number turbulent flow

2.1 A method of determination of the kernel G

As pointed out in references [28,40], the WT provides a powerful mathematical framework for analyzing irregular signals in both space and scale without loss of information. The WT of the turbulent velocity spatial field v at point x and scale $a > 0$, is defined as [41,42]:

$$T_\psi[v](x,a) = \frac{1}{a} \int_{-\infty}^{+\infty} v(y)\, \psi\left(\frac{x-y}{a}\right) \mathrm{d}y, \qquad (3)$$

where ψ is the analyzing wavelet. Note that the velocity increment $\delta v_l(x)$ is nothing else than $T_\psi[v](x,l)$ computed with the "poor man's" wavelet $\psi^{(1)}_{(0)}(x) = \delta(x-1) - \delta(x)$. More generally, ψ is chosen to be well localized not only in direct space but also in Fourier space (the scale a can thus

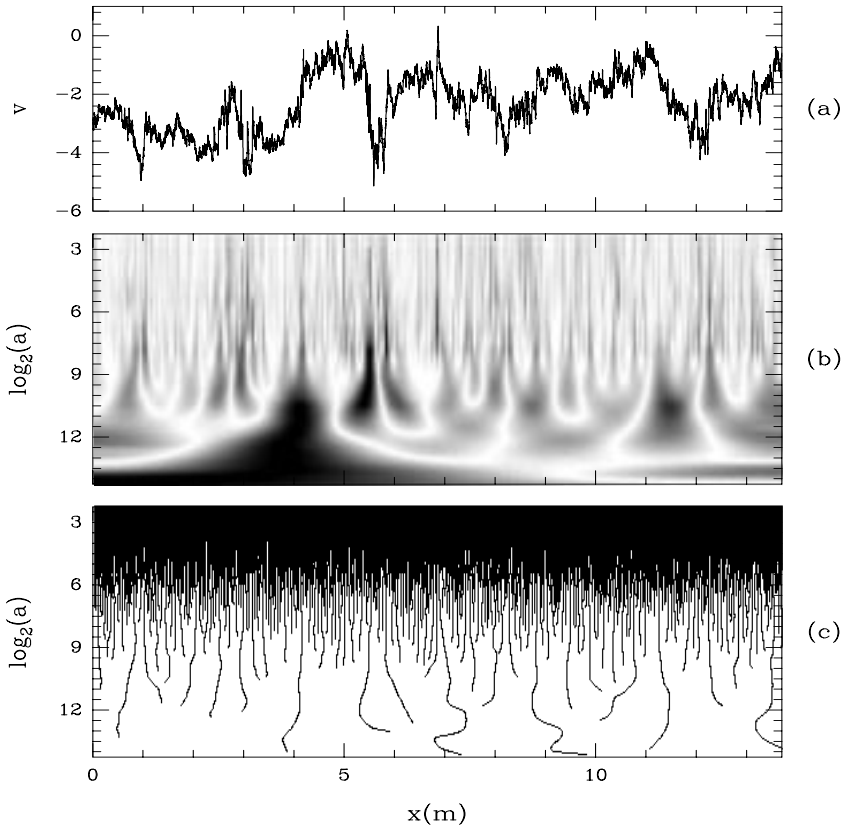

Fig. 1. Continuous WT of fully developed turbulence data from wind tunnel experiment. (a) The turbulent velocity signal over about two integral scales. (b) WT of the turbulent signal; the amplitude is coded, independently at each scale a, using 32 grey levels from white ($|T_\psi[v](x,a)| = 0$) to black ($\max_x |T_\psi[v](x,a)|$). (c) WT skeleton defined by the set of all the WTMM lines. In (b) and (c), the small scales are at the top. The analyzing wavelet is $\psi^{(1)}_{(3)}$.

be seen as the inverse of a local frequency). Throughout this study, we will use the set of compactly supported analyzing wavelets $\psi^{(n)}_{(m)}$ defined in references [37,39]. $\psi^{(1)}_{(m)}$ are smooth versions of $\psi^{(1)}_{(0)}$ obtained after m successive convolutions with the box function χ. $\psi^{(n)}_{(m)}$ are higher-order analyzing wavelets with n vanishing moments. The WT associates to a function in $\mathbb{R}$, its transform defined on $\mathbb{R}\times\mathbb{R}^+$ and is thus very redundant. Along the line of the strategy proposed in reference [37], we restrict our analysis to the *modulus maxima* of the WT (WTMM) so that the amount of data to process is more tractable (see Fig. 1). A straightforward generalization of equation (2) in terms of the WTMM pdf at scale a, $P_a(T)$, then reads

$$P_a(T) = \int G_{aa'}(u)\, P_{a'}(\mathrm{e}^{-u}T)\,\mathrm{e}^{-u}\mathrm{d}u, \text{ for } a' > a, \quad (4)$$

where for any decreasing sequence of scales $(a_1,\ldots,a_n)$, the kernel G satisfies the composition law:

$$G_{a_n a_1} = G_{a_n a_{n-1}} \otimes \cdots \otimes G_{a_2 a_1}, \quad (5)$$

where $\otimes$ denotes the convolution product. According to Castaing *et al.* [11,21], the cascade is *self-similar* if there exists a decreasing sequence of scales $\{a_n\}$ such that $G_{a_n a_{n-1}} = G$ is independent of n. The cascade is said continuously self-similar [11,21] if there exists a positive, decreasing function $s(a)$, such that $G_{aa'}$ depends on a and a' only through $s(a,a') = s(a) - s(a')$: $G_{aa'}(u) = G(u, s(a,a'))$. $s(a,a')$ actually accounts for the number of elementary cascade steps from scale a' to scale a ($s(a)$ can be seen as the number of cascade steps from the integral scale L down to the considered scale a). In the Fourier space, the convolution property (Eq. (5)) turns into a multiplicative property for $\widehat{G}$, the Fourier transform of G:

$$\widehat{G}_{aa'}(p) = \widehat{G}(p)^{s(a,a')}, \quad \text{for } a' > a. \quad (6)$$

From this equation, one deduces that $\widehat{G}$ has to be the characteristic function of an infinitely divisible pdf. Such a cascade is referred to as a log-infinitely divisible cascade [18–21]. According to Novikov's definition [18], the cascade is *scale-similar* (or *scale-invariant*) if

$$s(a,a') = \ln\left(\frac{a'}{a}\right), \quad (7)$$

i.e. $s(a) = \ln(L/a)$. Let us note that in their original work, Castaing *et al.* [11] have developed a formalism, based on an extremum principle, which is consistent with KO62 [13, 15] general ideas of log-normality and which predicts an anomalous power-law behavior of the depth of the cascade $s(a) \sim (L/a)^\beta$. From the computation of the scaling behavior of the variance of the kernel $G_{aa'}$, they have checked that the above mentioned power-law behavior could provide a reasonable explanation for the deviation from scaling observed experimentally on the velocity fluctuation statistics [11,29–33].

Our numerical estimation of G [37] is based on the computation of the characteristic function $M(p,a)$ of

the WTMM logarithms at scale a:

$$M(p,a) = \int \mathrm{e}^{ip\ln|T|} P_a(T)\,\mathrm{d}T. \tag{8}$$

From equation (4), it is easy to show that $\widehat{G}$ satisfies:

$$M(p,a) = \widehat{G}_{aa'}(p)\,M(p,a'). \tag{9}$$

After the WT calculation and the WTMM detection, the real and imaginary parts of $M(p,a)$ are computed separately as $\langle\cos(p\ln|T|)\rangle$ and $\langle\sin(p\ln|T|)\rangle$ respectively. The use of the WTMM skeleton instead of the continuous WT prevents $M(p,a')$ from getting too small as compared to numerical noise over a reasonable range of values of p, so that $\widehat{G}_{aa'}(p)$ can be computed from the ratio:

$$\widehat{G}_{aa'}(p) = \frac{M(p,a)}{M(p,a')}\cdot \tag{10}$$

We refer the reader to references [37,39] for test applications of this method to synthetic turbulent signals.

2.2 Experimental determination of the kernel G

The turbulence data were recorded by Gagne and collaborators in the S1 wind tunnel of ONERA in Modane. The Taylor scale based Reynolds number is about $R_\lambda \simeq 2000$ and the Kolmogorov $k^{-5/3}$ law for the energy spectrum approximately holds on an "inertial range" of about four decades (from the integral scale $L \simeq 7$ m down to the dissipative scale $\eta \simeq 0.27$ mm). The overall statistical sample is about 25×10^7 points long, with a resolution of roughly 3η, corresponding to about 25 000 integral scales. Temporal data are identified to spatial fluctuations of the longitudinal velocity *via* the Taylor hypothesis [4,9]. Figure 1 illustrates the WT and its skeleton, of a sample of the (longitudinal) velocity signal of length of about two integral scales. The analyzing wavelet $\psi^{(1)}_{(3)}$ is a first order compactly supported wavelet. We have checked that all the results reported below are consistent when changing both the regularity and the order of ψ.

2.2.1 Uncovering a continuously self-similar cascade

In order to test the validity of equation (6), we first focus on the scale dependence of $\widehat{G}_{aa'}$ as calculated with equation (10). Figures 2a and 2b respectively show the logarithm of the modulus $\ln|\widehat{G}_{aa'}|$ and the phase $\phi_{aa'}$ of $\widehat{G}_{aa'}$ for various pairs of scales $a < a'$ in the inertial range. In Figures 2c and 2d, we succeed in collapsing all different curves in Figures 2a and 2b onto a single kernel $\widehat{G} = \widehat{G}^{1/s(a,a')}_{aa'}$, in very good agreement with equation (6) and the continuously self-similar cascade picture.

In the inserts of Figures 2a and 2b, we compare our estimation of $\widehat{G}_{aa'}$ for the turbulent signal and for a log-normal numerical process of the same length generated using an algorithm of multiplicative cascade defined on an orthonormal wavelet basis [43]. The main lines of this generator of synthetic turbulence are described in Appendix A. On the numerical log-normal cascade, deviations from the expected parabolic behavior of $\ln|\widehat{G}_{aa'}|$ as well as from the linear behavior of $\phi_{aa'}$ (see Eq. (14)), become perceptible for $|p| > 5$. Very similar features are observed for the turbulence data, showing that the slight dispersion at large values of p on the curves in Figures 2c and 2d can be attributed to a lack of statistics. Thus, from now on, we will restrict our analysis of $\widehat{G}(p)$ to $p \in [-4,4]$.

In order to collapse all the curves on a same one in both Figures 2c and 2d, we need to adjust $s(a,a')$ in a way which actually breaks scale-invariance (Eq. (7)) since $s(a,a')$ is found to display some weak nonlinear dependence in $\ln(a'/a)$. Instead $s(a,a')$ turns out to be very well fitted by the functional form:

$$s(a,a') = \frac{a^{-\beta} - a'^{-\beta}}{\beta}, \tag{11}$$

where the exponent $\beta \simeq 0.095$ somehow quantifies the departure from scale-similarity (scale-invariance being restored for $\beta \to 0$). We refer the reader to references [37–39] for quantitative results on the breaking of scale-invariance in different flow configurations. Let us note that equation (11) differs from the pure power-law prompted by Castaing *et al.* [11,29–33], since when fixing the reference scale a', the number of cascade steps required to reach the scale a is not $a^{-\beta}/\beta$ but some corrective constant term $-a'^{-\beta}/\beta$ has to be taken into account.

2.2.2 Discriminating between log-normal and log-Poisson cascades

The relevance of equation (6) being established, let us turn to the precise analysis of the nature of G. Using the Taylor series expansion of $\ln\widehat{G}(p)$:

$$\widehat{G}(p) = \exp\left(\sum_{k=1}^{\infty} c_k \frac{(\mathrm{i}p)^k}{k!}\right), \tag{12}$$

equation (6) can be rewritten as:

$$\widehat{G}_{aa'}(p) = \exp\left(\sum_{k=1}^{\infty} s(a,a')\,c_k \frac{(\mathrm{i}p)^k}{k!}\right), \tag{13}$$

where the (real valued) coefficients c_k are the cumulants of G.

- Log-normal cascade process [13,15]: a log-normal cascade is characterized by a Gaussian kernel [37,39]:

$$\widehat{G}_{aa'}(p) = \exp\left[s(a,a')\left(-imp - \sigma^2\frac{p^2}{2}\right)\right], \tag{14}$$

which corresponds to the following set of cumulants:

$$c_1 = -m\ ,\ c_2 = \sigma^2 \ \text{ and } \ c_k = 0 \ \text{ for } \ k \geq 3. \tag{15}$$

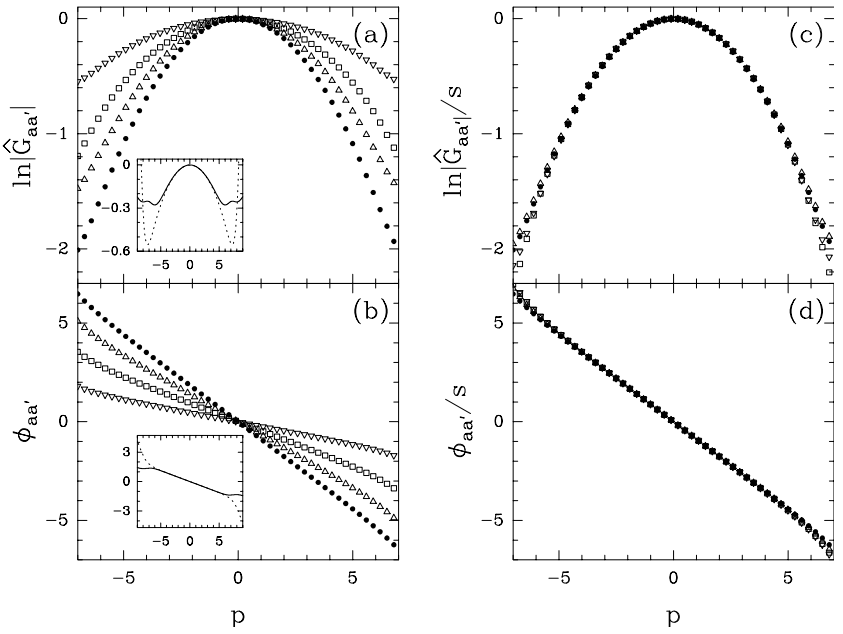

Fig. 2. Estimation of $\widehat{G}_{aa'}(p)$ for the Modane turbulent velocity signal ($R_\lambda \simeq 2000$) using equation (10). The analyzing wavelet is $\psi^{(1)}_{(3)}$. (a) $\ln|\widehat{G}_{aa'}(p)|$ *versus* p; (b) $\phi_{aa'}(p)$ *versus* p for $a = 271\eta$, $a' = 4340\eta$ (•), $a = 385\eta$, $a' = 3080\eta$ (△), $a = 540\eta$, $a' = 2170\eta$ (□), $a = 770\eta$, $a' = 1540\eta$ (▽). Inserts: the experimental $\widehat{G}_{aa'}(p)$ for $a = 770\eta$ and $a' = 1540\eta$ (dotted line) compared to the computation of $\widehat{G}_{aa'}(p)$ for a log-normal numerical process (Appendix A) of parameters $m = 0.32$ and $\sigma^2 = 0.03$ with $a = 2^8$ and $a' = 2^9$ (solid line). (c) and (d) The same curves after being rescaled by a factor $1/s(a, a')$ with $s = 1$ (•), $s = 0.754$ (△), $s = 0.508$ (□), $s = 0.254$ (▽).

- Log-Poisson cascade process [19–22]: a log-Poisson cascade is characterized by the following kernel shape [37,39]:

$$\widehat{G}_{aa'}(p) = \exp[s(a,a')(\lambda(\cos(p\ln\delta) - 1) + i(p\gamma + \lambda\sin(p\ln\delta)))], \quad (16)$$

where λ, δ and γ are parameters. This log-Poisson kernel corresponds to the following set of cumulants:

$$c_1 = \gamma + \lambda\ln\delta \;\text{ and }\; c_k = \lambda(\ln\delta)^k \;\text{ for }\; k \geq 2. \quad (17)$$

Note that the log-Poisson process reduces to a log-normal cascade for $|p\ln\delta| \ll 1$, *i.e.*, in the limit $\delta \to 1$ and $\lambda(\ln\,\delta)^2 \to \sigma^2$ where the atomic nature of the quantized log-Poisson process vanishes.

For a given pair of inertial scales $a < a'$, we proceed to polynomial fits of $\ln|\widehat{G}_{aa'}(p)|$ and $\phi_{aa'}(p)$, prior to the use of equation (13) to estimate the first three cumulants $C_k = s(a,a')\,c_k$ as a function of the statistical sample length for the turbulence data and for both a log-normal and a log-Poisson synthetic numerical processes. Figure 3 shows that statistical convergence is achieved up to the third order coefficient. For higher order cumulants, however, our sample total length does not allow an acceptable convergence. The m and σ^2 parameters of the log-normal process inferred from the asymptotic values of C_1 and C_2 (Figs. 3a, b), namely $m = 0.32$ and $\sigma^2 = 0.03$, lead to a very small numerical third order coefficient that cannot be distinguished from the experimental C_3 (Fig. 3c). In the log-Poisson model, by setting $\lambda = 2$ (according to She and Leveque [22], λ is the codimension of the most intermittent structures that are assumed to be filaments), we were able to find values of δ and γ close to those proposed in reference [22] ($\delta = (2/3)^{1/3}$ and $\gamma = -1/9$), that perfectly fit the first two cumulants. However, as seen in

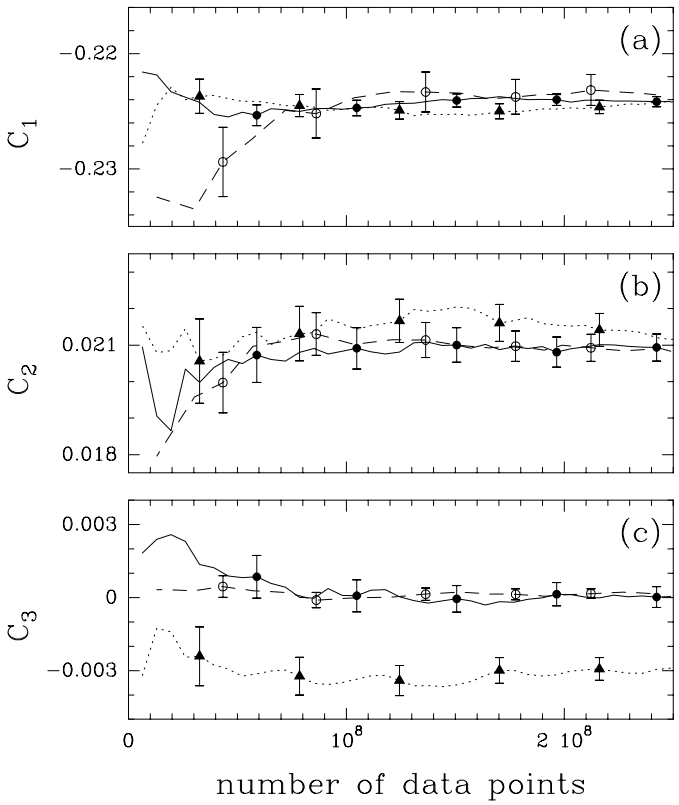

Fig. 3. The first three cumulants of $G_{aa'}$ *versus* the sample length. Turbulent velocity signal for $a = 770\eta$ and $a' = 1540\eta$ (○ and dashed line), log-normal numerical process of parameters $m = 0.32$ and $\sigma^2 = 0.03$ (• and solid line) and log-Poisson numerical process of parameters $\lambda = 2$, $\delta = 0.89$ and $\gamma = -0.082$ (▲ and dots) for the two corresponding scales $a = 2^8$ and $a' = 2^9$. Numerical processes are scale-invariant (see Appendix A) so that $C_k = \ln 2 \cdot c_k$. Error bars are estimates of the r.m.s. deviations of the cumulants from their asymptotical values.

Figure 3c, this set of parameters yields a third order cumulant that is more than one order of magnitude higher than the experimental one. Actually, when taking λ as a free parameter, good log-Poisson approximations of all the first three cumulants are obtained for unrealistic values of λ of order 100 and for values of δ very close to 1, *i.e.*, when the log-Poisson process reduces to the log-normal model. From these results, we conclude that, for the analyzed wind tunnel velocity signal ($R_\lambda \simeq 2000$), G is a Gaussian kernel since $C_k = 0$ implies $c_k = 0$ for $k > 2$. The large size of our statistical sample allows us to exclude log-Poisson statistics with the parameters proposed in reference [22].

3 Experimental tests of the validity of log-normal statistics

3.1 WTMM probability density functions

A first way to check the consistency of our results is to test the convolution formula (4) on the WTMM pdf's using a Gaussian kernel. The results of this test application are reported in Figure 4. Let us mention that a naive computation of the pdf's of the (continuous) WT coefficients at different scales in the inertial range [39], leads to distributions that are nearly centered with a shape that goes from Gaussian at large scales to stretched exponential-like tails at smaller scales, very much like the evolution observed for the velocity increment pdf's [4,8,11,34–36]. But the wavelet theory [41,42] tells us that there exists some redundancy in the continuous WT representation. Indeed, for a given analyzing wavelet, there exists a reproducing kernel [44,45] from which one can express any WT coefficient at a given point x and scale a as a linear combination of the neighboring WT coefficients in the space-scale half-plane. As emphasized in references [40,46,47], a way to break free from this redundancy is to use the WTMM representation. In Figure 4a are reported the results of the computation of the WTMM pdf's when restricting our analysis to the WT skeleton (Fig. 1c) defined by the WT maxima lines. Since by definition the WTMM are different from zero, the so-obtained pdf's decrease exponentially fast to zero at zero, which will make the estimate of the exponents ζ_q tractable for $q < 0$ in Section 3.2. When plotting $\ln P_a(\ln(|T|))$ *versus* $\ln|T|$, one gets in Figure 4b the remarkable result that for any scale in the inertial range, all the data points fall, within a good approximation, on a parabola, which is a strong indication that the WTMM have a log-normal distribution. In Figure 4c, we have succeeded in collapsing all the WTMM pdf's, computed at different scales, onto a single curve when using equation (4) with a Gaussian kernel $G(u, s(a,a'))$ where $s(a,a')$ is given by equation (11) with $\beta = 0.095$ in order to account for the scale-invariance breaking mentioned above (Sect. 2.2.1). This observation corroborates the log-normal cascade picture. Let us point out that, as illustrated in Figures 4c and 4d, the velocity increment pdf's are likely to satisfy the Castaing *et al.* convolution formula (2) with a similar Gaussian kernel, even though their shape evolves across the scales [39]. The fact that the WTMM pdf's turn out to have a shape which is the fixed point of the underlying kernel has been numerically revealed in previous works [37,39] for various synthetic log-infinitely divisible cascade processes.

3.2 ζ_q scaling exponents

A second test of the log-normality of the velocity fluctuations lies in the determination of the ζ_q spectrum. As discussed in previous studies [40,48], the structure function approach pioneered by Frisch and Parisi [23] has several intrinsic insufficiencies which mainly result from the poorness of the underlying analyzing wavelet $\psi^{(1)}_{(0)}$. Here we use instead the so-called WTMM method [28,40,47,48] that has proved to be very efficient to achieve multifractal analysis of very irregular signals. The WTMM method consists in computing the following partition functions:

$$Z(q,a) = \sum_{l \in \mathcal{L}(a)} \left(\sup_{\substack{(x,a') \in l \\ a' \leq a}} |T_\psi[v](x,a')| \right)^q , \quad \forall q \in \mathbb{R}, \tag{18}$$

where $\mathcal{L}(a)$ denotes the set of all WTMM lines of the space-scale half-plane that exist at scale a and contain maxima at any scale $a' \leq a$. A straightforward analogy with the structure functions $S_q(l)$ (Eq. (1)) yields:

$$\mathcal{S}(q,a) \stackrel{\text{def}}{=} \frac{Z(q,a)}{Z(0,a)} \sim a^{\zeta_q}. \tag{19}$$

However, there exist two fundamental differences between $S_q(l)$ and $\mathcal{S}(q,a)$. (i) The summation in equation (18) is over the WT skeleton defined by the WTMM. Since by definition the WTMM do not vanish, equation (18) allows us to extend the computation of the scaling exponents ζ_q from positive q values only when using the structure functions (as shown in Sect. 3.1, the velocity increment pdf's do not vanish at zero), to positive as well as negative q values without any risk of divergences [48]. (ii) By considering analyzing wavelets that are regular enough and with some adjustable degree of oscillation, the WTMM method allows us to capture singularities in the considered signal ($0 \leq h \leq 1$) like the structure functions can do, but also in arbitrary high order derivatives of this signal [40]. In that respect, the WTMM method gives access to the entire $D(h)$ singularity spectrum and not only to the strongest singularities as the structure function method is supposed to do from Legendre transforming ζ_q for $q > 0$ only [28, 40,47,48].

Since scale-invariance is likely to be broken, one rather expects the more general scale dependence of $\mathcal{S}(q,a)$ [37–39]:

$$\mathcal{S}(q,a) = \kappa_q \exp(-\zeta_q s(a)), \tag{20}$$

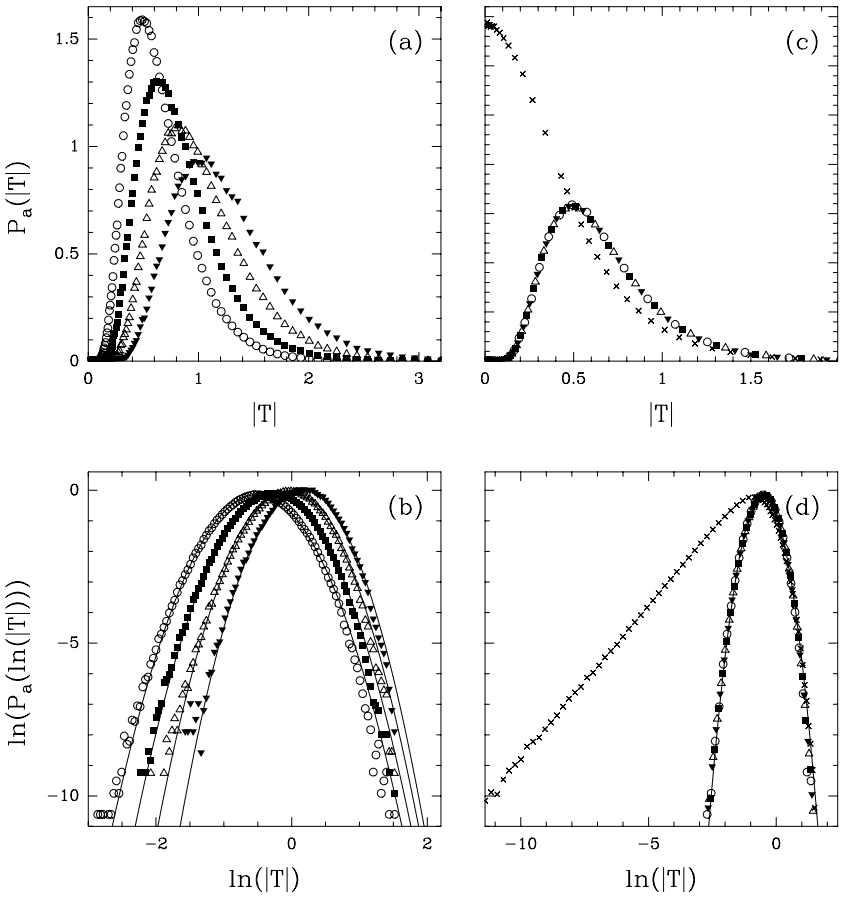

Fig. 4. Probability density functions of the WTMM for the Modane turbulent velocity signal. (a) $P_a(|T|)$ *versus* $|T|$ as computed at different scales $a = 385\eta$ (○), 770η (■), 1540η (△) and 3080η (▼). (b) $\ln(P_a(\ln(|T|)))$ *versus* $\ln|T|$ at the same scales. (c) and (d) The pdf's after being transformed according to equation (4) with a Gaussian kernel $G_{aa'}$ and $s(a,a') = (a^{-\beta} - a'^{-\beta})/\beta$ where $\beta = 0.095$. The (×) in (c) and (d) represent the velocity increment pdf at scale $a = 308\eta$. The solid lines in (b) and (d) correspond to the Gaussian approximations of the histograms. The analyzing wavelet is $\psi^{(1)}_{(3)}$.

where κ_q is a constant that depends only on q and $s(a) = (a^{-\beta} - 1)/\beta$ consistently with the observed anomalous behavior of $s(a,a')$ given by equation (11). Indeed, $\mathcal{S}(q,a)$ can be seen as a mean of $|T|^q$ so that formally, from the definition of the characteristic function $M(q,a)$ (Eq. (8)), one gets:

$$\mathcal{S}(q,a) \sim M(-iq,a). \tag{21}$$

From the expression (10) of the Fourier transform of the kernel G and equation (21), one deduces:

$$\frac{\mathcal{S}(q,a)}{\mathcal{S}(q,a')} = \widehat{G}_{aa'}(-iq). \tag{22}$$

When further using equation (13), this last equation becomes:

$$\frac{\mathcal{S}(q,a)}{\mathcal{S}(q,a')} = \exp\left(\sum_{k=1}^{\infty} s(a,a')\, c_k \frac{q^k}{k!}\right) \tag{23}$$

which is consistent with equation (20) provided

$$\zeta_q = -\sum_{k=1}^{\infty} c_k q^k/k! \ . \tag{24}$$

We have checked that fitting $\mathcal{S}(q,a)/\mathcal{S}(q,a')$ *versus* q for the two scales of Figure 3, leads to the same estimates of $C_k = s(a,a')\, c_k$ as above within less than 1%.

Remarks: (i) Let us emphasize that for $\psi = \psi^{(1)}_{(0)}$, equation (20) is nothing but the general exponential self-similar behavior predicted by Dubrulle [49] (for the structure functions) by simple symmetry considerations. (ii) As expressed by equation (20), the observed breaking of scale-invariance does not invalidate ESS hypothesis [25–27]. Actually, one should better say that equation (20) provides some validation of ESS.

To estimate the ζ_q spectrum, we thus use the concept of ESS developed by Benzi *et al.* [25–27], *i.e.*, we set $\zeta_3 = 1$ and plot $\mathcal{S}(q,a) = (\kappa_q/\kappa_3)\mathcal{S}(3,a)^{\zeta_q}$ *versus* $\mathcal{S}(3,a)$ in log-coordinates (for more details see Ref. [38]). As shown in Figure 5a, the experimental spectrum obtained from linear regression procedure, remarkably coincides with the quadratic log-normal prediction $\zeta_q = mq - \sigma^2 q^2/2$ with the same parameters as in Section 2.2.2 (Fig. 3), up to $|q| = 10$. We have checked that statistical convergence is achieved for $|q| \leq 8$; but even if the convergence becomes questionable for larger values of q, the "error bars" obtained by varying the range of scales used for the ESS determination of ζ_q show the robustness of the spectrum. Let us point out that the log-Poisson prediction $\zeta_q = -\gamma q + \lambda(1 - \delta^q)$, with the She and Leveque [22] parameter values: $\lambda = 2$, $\delta = (2/3)^{1/3}$ and $\gamma = -1/9$, provides a rather good approximation of ζ_q for $q \in [-6,6]$, in agreement with the structure function estimations of ζ_q [10, 20,22,36] and with our results on the first two cumulants

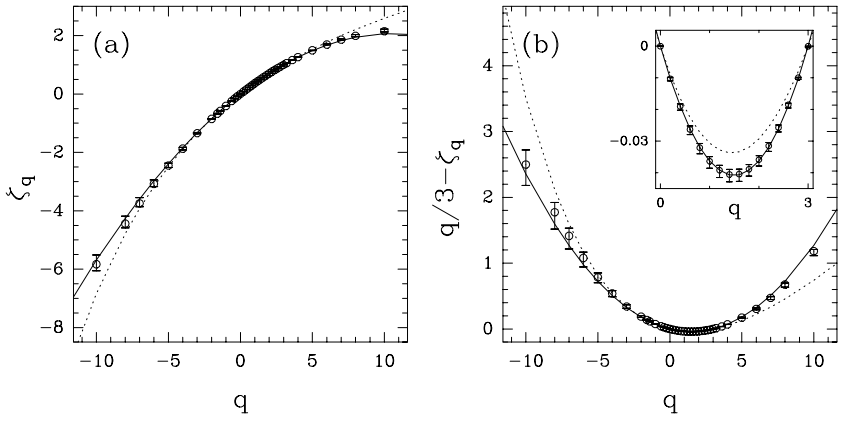

Fig. 5. WTMM estimation of the ζ_q spectrum for the Modane turbulent velocity signal. The analyzing wavelet is $\psi^{(1)}_{(3)}$. (a) ζ_q *versus* q. (b) Deviation of the experimental spectrum from the K41 $\zeta_q = q/3$ prediction. The experimental measurements (○) are compared to the theoretical quadratic ESS spectrum of a log-normal process with $m = 0.32$ and $\sigma^2 = 0.03$ (solid line) and to the She and Leveque [22] log-Poisson prediction with $\lambda = 2$, $\delta = (2/3)^{1/3}$ and $\gamma = -1/9$ (dots).

of G (Fig. 3). However, plotting the deviation of the ζ_q's from the K41 linear $\zeta_q = q/3$ spectrum (Fig. 5b), reveals a systematic departure of the log-Poisson prediction from the experimental spectrum, and this even for $q \in [0, 3]$ as shown in the insert of Figure 5b, whereas the log-normal model still perfectly fits the experimental data. This nicely corroborates our findings on the third order cumulant of G (Fig. 3) and shows that very long statistical samples are needed to discriminate between log-normal and log-Poisson statistics in fully developed turbulence data. Note that according to the quadratic fit reported in Figure 5, the ζ_q spectrum should decrease for $q \geq 11$, in qualitative agreement with previous discussions [11,36]. However, since statistical convergence is not achieved for such high values of q, one has to be careful when extrapolating the ζ_q behavior. As reported in reference [36], the number of data points needed to estimate ζ_q increases exponentially fast with q. Reaching an acceptable statistical convergence for $q \simeq 12$ would thus require velocity records about ten times bigger than those processed in this work.

4 Discussion

To complete our study, we shall now try to answer two important questions. (i) What is the extent of the scale range where the statistics can be considered as log-normal? (ii) Do our results still hold when the Reynolds number is varied?

4.1 Defining an inertial range

As pointed out in references [8–11,36,50,51], the so-called "inertial range", on which structure functions approximately follow a power law behavior, is narrower than $[\eta, L]$. Actually, because of scale-invariance breaking [37–39], such an "inertial range" is not well defined and might even not exist. Thus, we may rather call "inertial range" the range of scales on which equation (6) holds with the same kernel G. The extent of the inertial range may then be estimated using the following quantity:

$$h(q,a) = \frac{\partial \ln Z}{\partial q}(q,a) = \frac{\partial \ln \mathcal{S}}{\partial q}(q,a), \qquad (25)$$

from which one can define the following test function:

$$H(q,a) = h(0,a) - \frac{1}{2}\left(h(q,a) + h(-q,a)\right). \qquad (26)$$

Indeed, using equation (20), it is easy to establish that, if G is a symmetric distribution around its mean value $m = -c_1$ (*i.e.* $c_{2k+1} = 0$ for all $k \geq 1$), then $H(q,a)$ is independent of a and is given by

$$H(q,a) = H_q = \frac{\partial \ln \kappa_q}{\partial q}(0) + \frac{1}{2}\left(\frac{\partial \ln \kappa_q}{\partial q}(q) + \frac{\partial \ln \kappa_q}{\partial q}(-q)\right). \qquad (27)$$

Figure 6 shows that, for different values of q, $H(q,a)$ is scale independent over an inertial range that extends from $a \simeq 300\eta$ to $a \simeq 8000\eta$. Since the log-Poisson distribution is not symmetric, this result constitutes an additional argument in favor of log-normal statistics. Moreover, the observation that the plateau value H_q scales like q^2 is in agreement with equation (27) that generically predicts a quadratic behavior of H_q, at least for small values of q.

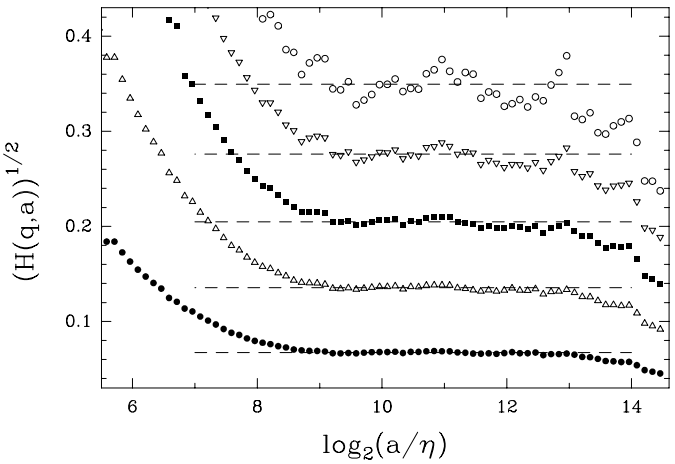

Fig. 6. $(H(q,a))^{1/2}$ *versus* $\log_2(a/\eta)$ for different values of q: $q = 1$ (●), 2 (△), 3 (■), 4 (▽) and 5 (○). The dashed lines represent the plateau values H_q which scale like q^2.

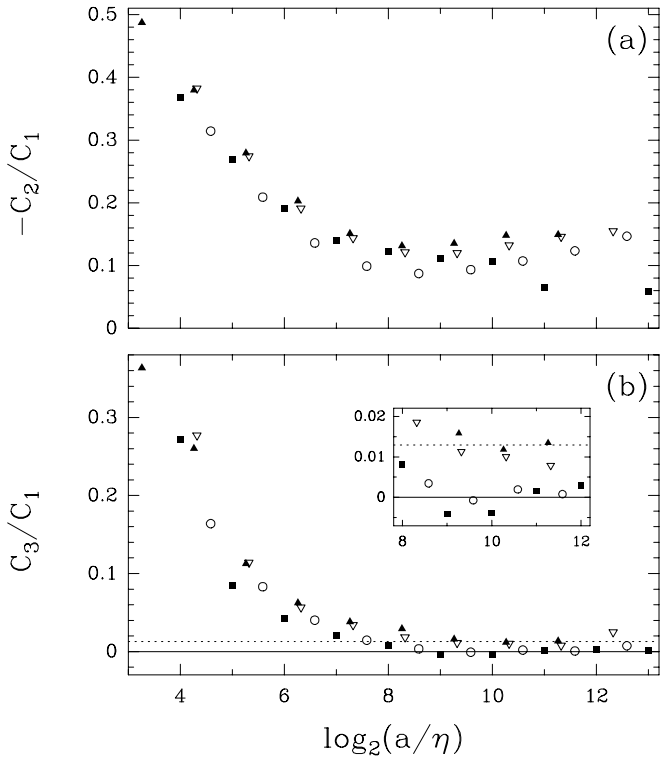

Fig. 7. Cumulant ratios $-C_2/C_1$ (a) and C_3/C_1 (b), estimated from $\widehat{G}_{aa'}$ with $a' = 2a$, as a function of $\log_2(a/\eta)$ for four turbulent flows of different Reynolds numbers $R_\lambda \simeq 2000$ (○), 800 (▽), 600 (▲) and 280 (■). In (b), the solid and dotted lines correspond respectively to the log-normal and to the She and Leveque [22] log-Poisson predictions for C_3/C_1.

In Figure 7 are reported the results of the computation of the ratios $-C_2/C_1$ and C_3/C_1 from $\widehat{G}_{aa'}(p)$ for all available scales a and $a' = 2a$. In spite of a small increase of $-C_2/C_1 \simeq 0.1$ at large scales, the shape of the kernel $G_{aa'}$ remains remarkably constant over the range $[300\eta, 8000\eta]$ with values of C_3/C_1 very close to 0, so that the statistics can be considered as log-normal on the whole observed inertial range.

4.2 Investigating the dependence of the statistics on the Reynolds number

We have reproduced our WT-based analysis on a turbulent velocity signal at Reynolds number $R_\lambda \simeq 800$ (of about the same length as the previous statistical sample and with a resolution of 2.5η) obtained by Gagne *et al.* in a laboratory jet experiment. As illustrated in Figure 7, for $R_\lambda \simeq 800$, C_3/C_1 is significantly higher (of order 0.01) than for $R_\lambda \simeq 2000$, whereas $-C_2/C_1$ remains of order 0.15. An inertial range can still be defined, on which $G_{aa'}$ keeps a constant "inertial" shape, but for $R_\lambda \simeq 800$, this shape becomes compatible with a log-Poisson distribution as proposed in reference [22]. We have checked that in that case, the She and Leveque model provides a better approximation of the ζ_q spectrum than the log-normal model. This result seems in contradiction with previous studies

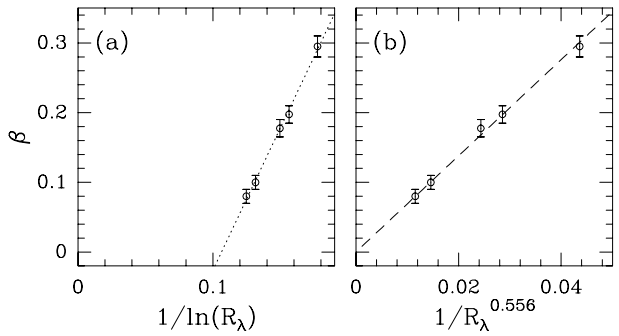

Fig. 8. β as a function of the Reynolds number. (a) β *versus* $1/\ln(R_\lambda)$; the dotted line corresponds to a fit of the data with $\beta = B(1/\ln(R_\lambda) - 1/\ln(R_\lambda^*))$ with $R_\lambda^* = 12000$. (b) β *versus* $R_\lambda^{-0.556}$; the dashed line corresponds to a linear regression fit of the data. Error bars account for variation of β according to the definition of the inertial range.

[10,36] suggesting that turbulent flows may be characterized by a universal ζ_q spectrum, independent of the Reynolds number, at least for $0 \leq q \leq 6$. However, as seen in Figure 5a, for that range of q values, the various models can hardly be distinguished without plotting $q/3 - \zeta_q$. From our WT-based approach, that allows the determination of ζ_q for negative q values, when using very long statistical samples to minimize error bars, we can actually conclude that log-normal statistics no longer provide a perfect description of the turbulent velocity signal at Reynolds number $R_\lambda \lesssim 800$. This result, together with previous numerical [52,53] and experimental [22,54] evidence for the relevance of log-Poisson statistics at low and moderate Reynolds numbers, strongly suggests that there might be some transitory regime ($R_\lambda \lesssim 1000$) towards asymptotic log-normal statistics, that could be accounted for by a quantized log-Poisson cascade or by some other cascade models that predict the correct relative order of magnitude of the higher order cumulants (mainly c_3 and c_4) of the kernel G (Eq. (12)).

In Figure 8 are reported the estimate of the scale breaking exponent β (Eq. (11)), as a function of the Reynolds number [38]; the five points correspond to the results obtained for the two previous experiments and for three additional data sets corresponding to wind tunnel ($R_\lambda \simeq 3050$), jet ($R_\lambda \simeq 600$) and grid ($R_\lambda \simeq 280$) turbulences. In Figure 8a, β is plotted *versus* $1/\ln(R_\lambda)$ in order to check experimentally the validity of some theoretical arguments developed in references [11,49], which predict a logarithmic decay of β when increasing R_λ. Indeed the data are very well fitted by $\beta \sim 1/\ln(R_\lambda) - 1/\ln(R_\lambda^*)$, where $R_\lambda^* \simeq 12000$, which suggests that scale-similarity is likely to be attained at finite Reynolds numbers. However, as shown in Figure 8b, for the range of Reynolds numbers accessible to today experiments, the data are equally very well fitted by a power-law decay with an exponent which is close to 1/2: $\beta \simeq R_\lambda^{-0.556}$. This second possibility brings the clue that scale-similarity might well be valid only in the limit of infinite Reynolds number. Whatever the relevant β behavior, our findings for the kernel $G_{aa'}$ at $R_\lambda \simeq 2000$ (high statistics in the present work) and

3050 (moderate statistics in Refs. [37,38]), strongly indicate that at very high Reynolds numbers, the intermittency phenomenon can be understood in terms of a continuous self-similar multiplicative process that converges towards a scale-similar log-normal cascade.

Let us note that in Figure 7b, the estimate of C_3/C_1 for the lowest Reynolds number velocity signal ($R_\lambda \simeq 280$) we have at our disposal cannot be distinguished from the results obtained for the wind-tunnel experiment at $R_\lambda \simeq 2000$. This observation of log-normal statistics at low Reynolds number contradicts the above conclusions. This might well be the consequence of the presence of some anisotropy at large scales in this grid turbulence where the velocity increment pdf's were found to depart significantly from a symmetric Gaussian shape [55].

5 Conclusions and perspectives

This study has revealed the existence of a scale domain that we call "inertial range", where a high Reynolds number turbulent velocity signal ($R_\lambda \simeq 2000$) displays log-normal statistics. Our results confirm the relevance of the continuously self-similar log-normal cascade picture initiated by Castaing *et al.* [11,21,29–33]. We also emphasize the fact that such an analysis requires very long statistical samples in order to get a good convergence of the cumulants of the kernel G and of the ζ_q spectrum. Our last results about the dependence of the statistics on the Reynolds number suggest that perfect log-normality may be reached only for $R_\lambda \to \infty$. A similar result is obtained concerning the breaking of scale-invariance [37–39]: scale-invariance is likely to be restored only for very large Reynolds numbers. As emphasized by Frisch [4], scale-invariance together with log-normal statistics for the velocity fluctuations imply that the Mach number of the flow increases indefinitely which violates a basic assumption needed in deriving the incompressible Navier-Stokes equations. Let us note that this observation does not, however, violate the basic laws of hydrodynamics since it is conceivable that, at extremely high Reynolds numbers, supersonic velocity may appear. A systematic investigation of the evolution of the statistics with both the scale range and the Reynolds number is currently under progress. Further analysis of numerical and experimental data should provide new insights on the departure of $G_{aa'}$ from its "inertial" shape outside the inertial range and on the way it converges towards a Gaussian kernel at high Reynolds numbers.

Beyond this "one-point" approach, a "two-point" statistical analysis of turbulent signals involving space-scale correlation functions looks very promising. In a preliminary work [56], we have proposed a method, based on the WT, which has proved to be particularly well suited to study multiplicative random cascade processes for which the correlation functions take a very simple form. This method has already been tested on various log-infinitely divisible cascade models and preliminarly applied to high Reynolds number turbulent velocity signals [56] and financial time series [57]. Further developments in the context of fully developed turbulence are in current progress.

We are very grateful to Y. Gagne and Y. Malecot for the permission to use their experimental turbulent signals. We acknowledge very stimulating discussions with E. Bacry, B. Castaing, S. Ciliberto, Y. Couder, S. Douady, B. Dubrulle, Y. Gagne, F. Graner, Y. Malecot, J.F. Pinton, P. Tabeling and H. Willaime. This work was supported by "Direction des Recherches, Études et Techniques" under contract (DRET n° 95/111).

Appendix A: Synthetic turbulence on orthonormal wavelet basis

We present a method of construction of scale-invariant signals using orthonormal wavelet basis [41,42]. This method allows us to generate measures as well as functions from a given deterministic or probabilistic multiplicative cascade process.

Let us consider the set $\{\psi_{j,k}\}$ of periodic wavelets that form an orthonormal basis of $\mathbb{L}^2([0,L])$. Thus $\forall f \in \mathbb{L}^2([0,L])$, f can be written under the form:

$$f(x) = \sum_{j=0}^{+\infty} \sum_{k=0}^{2^{j-1}} \langle \psi_{j,k} | f \rangle \, \psi_{j,k}(x) = \sum_{j=0}^{+\infty} \sum_{k=0}^{2^{j-1}} d_{j,k} \, \psi_{j,k}(x), \tag{A.1}$$

where

$$\psi_{j,k}(x) = 2^{j/2} \psi(2^{-j}x - k). \tag{A.2}$$

The set of coefficients $\{d_{j,k}\}$ therefore provides a complete characterization of the function f. Nowadays, there exists in the literature a wide range of possible choices of wavelet basis. Generally, this choice is dictated by the regularity of the signal one intends to synthetize. In the present study, we mainly use the Daubechies compactly supported wavelet basis [42] and more particularly the "Daubechies 9" basis generated from the highly regular functions $({}_9\phi,\ {}_9\psi)$ illustrated in Figures 10a and 10b respectively (${}_9\phi$ is the scale function and ${}_9\psi$ its conjugated wavelet).

The notion of cascade is then rather natural on the dyadic grid defined by the index (j,k). The construction rule is very similar to the one commonly used to generate self-similar measures [12,18,40], except that instead of redistributing the measure over sub-intervals with algebraic weight W, one allocates the wavelet coefficients $d_{j,k}$ in a multiplicative way on the dyadic grid. As illustrated in Figure 9, from an arbitrarily chosen value of the coefficient $d_{0,1}$, one generates the coefficients $d_{j,k}$, at successive scales, by iterating the following system:

$$\begin{cases} d_{j+1,2k} &= M_j^{(2)} \, d_{j,k} \,, \\ d_{j+1,2k+1} &= M_j^{(1)} \, d_{j,k} \,, \end{cases} \tag{A.3}$$

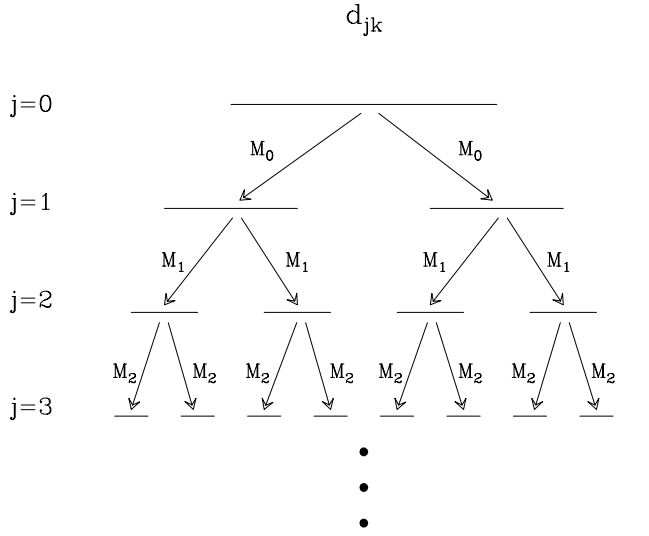

Fig. 9. Sketch of the construction rule of the wavelet coefficients $d_{j,k}$ on the dyadic grid, from the arbitrarily chosen coefficient $d_{0,1}$ using the hierarchical procedure defined in equation (A.3).

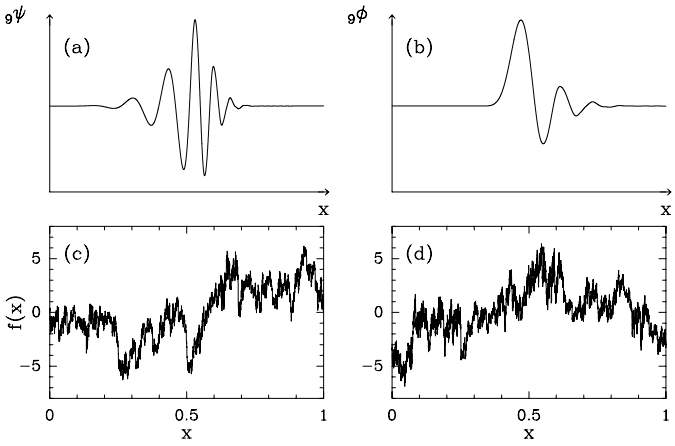

Fig. 10. Synthetic turbulent signals generated using the multiplicative construction rule illustrated in Figure 9 and the "Daubechies 9" compactly supported orthonormal wavelet basis [42]. (a) The mother wavelet ${}_9\psi$. (b) The corresponding scale function ${}_9\phi$ (we have arbitrarily set to zero the corresponding coefficients $c_{j,k} = 0$). (c) Log-Poisson cascade process with She and Leveque's model parameters $\lambda = 2$, $\delta = (2/3)^{1/3}$ and $\gamma = -1/9$. More precisely, $M = \mathrm{e}^{k \ln \delta + \gamma}$, where the random variable k obeys a Poisson law of mean $\lambda \ln 2$. (d) Log-normal cascade process with parameters $m = 0.32$ and $\sigma^2 = 0.03$.

where the $M_j^{(k)}$'s are realizations of a random variable M_j with prescribed law (which may possibly depend on j). The sign of $M_j^{(k)}$ is randomly decided at each iteration from "head and tail" game. Then, with the so-defined set of coefficients $d_{j,k}$, one uses equation (A.1) to construct a signal f from an appropriate wavelet basis. Let us point out that this synthetic signal can be qualified as self-similar in the sense that its wavelet coefficients result from a multiplicative cascade process. If the probability law of the M factors does not depend on j, this process is furthermore scale-invariant.

In Figures 10c and 10d are illustrated two turbulent synthetic signals generated respectively with a log-Poisson and a log-normal cascade process in order to mimic the experimental turbulent velocity signals recorded in the Modane wind tunnel (Fig. 1a). We refer the reader to references [43], for the mathematical demonstration that these cascade processes actually converge in some "reasonable" functional spaces with an adequate choice of the model parameters.

References

1. A.N. Kolmogorov, C.R. Acad. Sci. USSR **30**, 301 (1941).
2. A.S. Monin, A.M. Yaglom, *Statistical Fluid Mechanics* (MIT press, Cambridge, MA, 1975), Vol. 2.
3. U. Frisch, S.A. Orzag, Phys. Today, 24 (1990).
4. U. Frisch, *Turbulence* (Cambridge University Press, Cambridge, 1995).
5. M. Briscolini, P. Santangelo, S. Succi, R. Benzi, Phys. Rev. E **50**, R1745 (1994).
6. A. Vincent, M. Meneguzzi, J. Fluid Mech. **225**, 1 (1995).
7. F. Anselmet, Y. Gagne, E.J. Hopfinger, R.A. Antonia, J. Fluid Mech. **140**, 63 (1984).
8. Y. Gagne, Thesis, University of Grenoble (1987).
9. *Turbulence: A Tentative Dictionary*, edited by P. Tabeling, O. Cardoso (Plenum, New York, 1995).
10. A. Arneodo, *et al.*, Europhys. Lett. **34**, 411 (1996).
11. B. Castaing, Y. Gagne, E.J. Hopfinger, Physica D **46**, 177 (1990).
12. C. Meneveau, K.R. Sreenivasan, J. Fluid Mech. **224**, 429 (1991).
13. A.N. Kolmogorov, J. Fluid Mech. **13**, 82 (1962).
14. L. Richardson, Proc. R. Soc. London A **110**, 709 (1926).
15. A.M. Obukhov, J. Fluid Mech. **13**, 77 (1962).
16. D. Schertzer, S. Lovejoy, J. Geophys. Res. **92**, 9693 (1987).
17. S. Kida, J. Phys. Soc. Jpn **60**, 5 (1990).
18. E.A. Novikov, Phys. Fluids A **2**, 814 (1990); Phys. Rev. E **50**, 3303 (1995).
19. B. Dubrulle, Phys. Rev. Lett. **73**, 959 (1994).
20. Z.S. She, E.C. Waymire, Phys. Rev. Lett. **74**, 262 (1995).
21. B. Castaing, B. Dubrulle, J. Phys. II France **5**, 895 (1995).
22. Z.S. She, E. Leveque, Phys. Rev. Lett. **72**, 336 (1994).
23. U. Frisch, G. Parisi, in *Turbulence and Predictability in Geophysical Fluid Dynamics and Climate Dynamics*, edited by M. Ghil, R. Benzi, G. Parisi (North-Holland, Amsterdam, 1985), p. 84.
24. G. Pedrizetti, E.A. Novikov, A.A. Praskovsky, Phys. Rev. E **53**, 475 (1996).
25. R. Benzi, S. Ciliberto, R. Trippiccione, C. Baudet, F. Massaioli, S. Succi, Phys. Rev. E **48**, R29 (1993).
26. R. Benzi, S. Ciliberto, C. Baudet, G. Ruiz-Chavarria, R. Tripiccione, Europhys. Lett. **24**, 275 (1993).
27. R. Benzi, S. Ciliberto, C. Baudet, G. Ruiz-Chavarria, Physica D **80**, 385 (1995).
28. A. Arneodo, E. Bacry, J.F. Muzy, Physica A **213**, 232 (1995).
29. B. Castaing, Y. Gagne, M. Marchand, Physica D **68**, 387 (1993).

30. Y. Gagne, M. Marchand, B. Castaing, J. Phys. II France **4**, 1 (1994).
31. A. Naert, L. Puech, B. Chabaud, J. Peinke, B. Castaing, B. Hebral, J. Phys. II France **4**, 215 (1994).
32. B. Chabaud, A. Naert, J. Peinke, F. Chillà, B. Castaing, B. Hebral, *Phys. Rev. Lett.* **73**, 3227 (1994).
33. F. Chillà, J. Peinke, B. Castaing, J. Phys. II France **6**, 455 (1996).
34. P. Kailasnath, K.R. Sreenivasan, G. Stolovitzky, Phys. Rev. Lett. **68**, 2766 (1992).
35. P. Tabeling, G. Zocchi, F. Belin, J. Maurer, H. Willaime, Phys. Rev. E **53**, 1613 (1996).
36. F. Belin, P. Tabeling, H. Willaime, Physica D **93**, 52 (1996).
37. A. Arneodo, J.F. Muzy, S.G. Roux, J. Phys. II France **7**, 363 (1997).
38. A. Arneodo, S. Manneville, J.F. Muzy, S.G. Roux, Experimental evidence for anomalous scale dependent cascading process in turbulent velocity statistics, CRPP preprint (1997).
39. S.G. Roux, Ph D Thesis, University of Aix-Marseille II (1996).
40. J.F. Muzy, E. Bacry, A. Arneodo, Phys. Rev. Lett. **67**, 3515 (1991); Int. J. Bifurcation and Chaos **4**, 245 (1994).
41. Y. Meyer, *Ondelettes* (Hermann, Paris, 1990).
42. I. Daubechies, *Ten Lectures on Wavelets* (SIAM, Philadelphia, 1992).
43. (a) A. Arneodo, E. Bacry, S. Jaffard, J.F. Muzy, to appear in J. of Fourier Anal. and Appl. (1997); (b) A. Arneodo, E. Bacry, S. Manneville, J.F. Muzy, in preparation.
44. A. Grossmann, J. Morlet, SIAM J. Math. Anal. Appl. **15**, 723 (1984); in *Mathematics and Physics, Lecture on Recent Results*, edited by L. Streit (World Scientific, Singapore, 1985), p. 135.
45. I. Daubechies, A. Grossmann, Y. Meyer, J. Math. Phys. **27**, 1271 (1986).
46. S. Mallat, W.L. Hwang, IEEE Trans. Inform. Theory **38**, 617 (1992).
47. E. Bacry, J.F. Muzy, A. Arneodo, J. Stat. Phys. **70**, 635 (1993).
48. J.F. Muzy, E. Bacry, A. Arneodo, Phys. Rev. E **47**, 875 (1993).
49. B. Dubrulle, J. Phys. II France **6**, 1825 (1996).
50. C. Baudet, S. Ciliberto, P.N. Tien, J. Phys. II France **3** 293 (1993).
51. G. Stolovitzky, K.R. Sreenivasan, Phys. Rev. E **48**, R33 (1993).
52. E. Leveque, Z.S. She, Phys. Rev. Lett. **75**, 2690 (1995); Phys. Rev. E **55**, 2789 (1997).
53. R. Benzi, L. Biferale, E. Trovatore, Phys. Rev. Lett. **77**, 3114 (1996).
54. G. Ruiz-Chavarria, C. Baudet, S. Ciliberto, Phys. Rev. Lett. **74**, 1986 (1995).
55. Y. Gagne, Y. Malecot, private communication.
56. A. Arneodo, E. Bacry, S. Manneville, J.F. Muzy, Analysis of random cascades using space-scale correlation functions, CRPP preprint (1997).
57. A. Arneodo, J.F. Muzy, D. Sornette, Causal cascade in the stock market from the infrared to the ultraviolet, CRPP preprint (1997).